Research Square

Preprints are preliminary reports that have not undergone peer review.
They should not be considered conclusive, used to inform clinical practice,
or referenced by the media as validated information.

Self-organized circular polarization asymmetry in nonchiral random fiber lasers

Francesco Riboli

riboli@lens.unifi.it

National Research Council - National Institute of Optics (CNR-INO)

Wenyu Du

National Research Council - National Institute of Optics (CNR-INO)

Federico Tommasi

Università di Firenze https://orcid.org/0000-0002-3178-2514

Stefano Cavalieri

Dipartimento di Fisica e Astronomia, Università di Firenze, Via G. Sansone 1, Sesto, I-50019, Fiorentino, Italy

Diederik Wiersma

INRIM, Torino and University of Florence, Physics dept. and LENS https://orcid.org/0000-0001-8150-7425

Article

Keywords:

Posted Date: May 11th, 2026

DOI: https://doi.org/10.21203/rs.3.rs-9566356/v1

License: This work is licensed under a Creative Commons Attribution 4.0 International License.
Read Full License

Additional Declarations: There is no conflict of interest

Self-organized circular polarization asymmetry in nonchiral random fiber lasers

Wenyu Du[1], Federico Tommasi[2], Stefano Cavalieri[2], Diederik Sybolt Wiersma[3,2,4], Francesco Riboli[1,3,*]

[1]Istituto Nazionale di Ottica (INO), CNR, 50019 Sesto Fiorentino, Italy

[2]Dipartimento di Fisica e Astronomia, Università di Firenze, 50019 Sesto Fiorentino, Italy

[3]European Laboratory for Nonlinear Spectroscopy (LENS), 50019 Sesto Fiorentino, Italy

[4]Istituto Nazionale di Ricerca Metrologica (INRiM), 10135 Torino, Italy

Abstract

Random lasers are generally regarded as weakly polarized light sources because optical feedback is provided by multiple scattering rather than by well-defined cavities. Consequently, circular polarization in random lasers is commonly assumed to require intrinsically chiral materials or deliberately engineered chiral photonic structures. Whether circular polarization asymmetry can emerge spontaneously in a completely nonchiral random laser system remains an open question. Here, we report the emergence of pronounced circular polarization and clear circular polarization asymmetry in a nonchiral random laser based on polymer optical fibers doped with laser dye and scattering nanoparticles. Using full Stokes parameter measurements with spectral, spatial, and pump energy resolution, we show that circular polarization is absent in pure dye emission and below the lasing threshold, but appears abruptly once coherent random lasing feedback is established. The observed circular polarization is strongly mode and channel dependent, with different lasing modes exhibiting distinct magnitudes and even opposite handedness. Pump and wavelength resolved polarization maps and statistical analysis on the Poincare sphere demonstrate that circular polarization constitutes an independent degree of freedom selected by the disordered feedback network, demonstrating a self-organized emergence of circular polarization asymmetry driven primarily by disordered feedback. These results indicate that random lasers can behave as asymmetric optical cavities capable of generating circular polarization without material chirality, opening new routes for polarization control in disordered photonic systems.

Introduction

The concept of random lasing, in which optical feedback is provided by multiple scattering rather than conventional cavity mirrors, was first proposed by Letokhov in 1968. He theoretically predicted that a gain medium containing randomly distributed scatterers could support laser oscillation once the photon scattering mean free path became comparable to the gain length [1]. This prediction was experimentally verified several decades later by Lawandy and coworkers, who observed laser like emission from a strongly scattering dye solution, characterized by a clear threshold behavior and pronounced spectral narrowing [2]. Since then, random lasers have attracted sustained interest due to their simple cavity free architecture, rich physical mechanisms, and potential applications in areas such as imaging, sensing, and speckle free illumination [3-5]. Early investigations primarily focused on lasing thresholds, emission spectra, and coherence properties, establishing the fundamental characteristics of random lasing systems [6-9].

Because photons in random lasers undergo multiple scattering along highly disordered propagation paths, the emitted light was long assumed to be weakly polarized or completely unpolarized. As a result, polarization properties were often regarded as secondary features and were typically characterized only through simple intensity averages. Subsequent studies, however, revealed that polarization memory can survive under certain conditions. Knitter et al reported that random lasers in dye solutions can exhibit measurable linear polarization when pumped with linearly polarized light, particularly in gain media with anisotropic absorption [10]. Ye et al further showed that dye doped nematic liquid crystals support polarization dependent random lasing, where the birefringence and anisotropy of the host medium play a decisive role in shaping the emission polarization [11]. These results clearly indicate that polarization in random lasers is not purely randomized, but instead depends sensitively on gain anisotropy, scattering geometry, and excitation conditions[12].

In parallel with these developments, significant progress has been made in generating circularly polarized luminescence and circularly polarized lasing in chiral and anisotropic photonic systems. Chiral nematic liquid crystals have been widely explored because of their ability to selectively reflect one handedness of circularly polarized light while transmitting the opposite. This selective Bragg reflection enables the conversion of unpolarized fluorescence into strongly circularly polarized emission, with dissymmetry factors *g* approaching the theoretical limit of 2.0 [13], where $g=2(I_R-I_L)/(I_R+I_L)$, with I_R and I_L denoting the intensities of right- and left-handed circularly polarized emission, respectively. Similar effects have been achieved in cholesteric liquid crystal polymer networks, where tuning the film thickness and helical pitch allows the dissymmetry factor *g* to be enhanced from 0.7 to 1.6 through polarization selective feedback near the photonic band edge [14]. Hybrid chiral systems, such as metal organic frameworks with intrinsically chiral lattices, have also demonstrated circularly polarized luminescence, where asymmetric donor-acceptor energy transfer yields dissymmetry factors *g* on the order of 0.55 [15].

Notably, circular polarization can also be imposed on achiral emitters by embedding them in chiral optical environments. For example, achiral dyes dissolved in cholesteric liquid crystal hosts can produce wavelength dependent circular polarization through Forster resonance energy transfer combined with selective reflection [16]. Beyond spontaneous emission, circularly polarized stimulated emission has been reported in chiral cavity systems and polymer thin films exhibiting apparent circular dichroism. In these systems, polarization asymmetry accumulates through multiple reflections within the cavity, leading to circularly polarized lasing even when the gain medium itself is not intrinsically chiral [17]. Together, these studies demonstrate that circular polarization can arise either from molecular chirality or from deterministic polarization selective optical feedback imposed by chiral or periodically ordered structures.

In contrast to these well-defined systems, random lasers provide a fundamentally different platform in which optical feedback emerges from stochastic multiple scattering rather than from designed resonators. Nevertheless, most reported demonstrations of circularly polarized random lasing rely on explicitly introducing chirality through materials or photonic architectures. Directional and polarization selective random lasing has been achieved by engineering scattering paths or incorporating chiral scatterers, thereby bridging the gap between conventional cavity lasers and random systems [18]. A representative example is the random laser based on the scarab beetle elytral surface, where the naturally occurring chiral photonic structure leads to strongly angle dependent circular polarization, with luminescence dissymmetry factors reaching g 0.9 or -0.5 at specific observation angles [19]. In another approach, Lee and coworkers realized random lasing with pronounced circular dichroism by introducing chiral plasmonic gold nanoparticles into a dye scatterer mixture, reporting dissymmetry factors g as high as 0.23 once the random lasing network was established [20]. These results have reinforced the widespread assumption that material chirality is a necessary condition for achieving circular polarization asymmetry in random laser systems.

Motivated by these open issues, the central question addressed in this work is whether a fully nonchiral disordered feedback network can spontaneously select circular polarization states through random laser mode competition, rather than through predefined chiral materials or designed resonant structures. Here, we challenge the prevailing assumption that chirality is a prerequisite for circular polarization asymmetry. Figure 1 summarizes the physical framework of the present study and the key observables used to characterize polarization in the polymer optical fiber random laser system. We report that a high degree of circular polarization and pronounced handedness asymmetry can emerge in a completely nonchiral random laser system based on polymer optical fibers. Through comprehensive polarization analysis using all four Stokes parameters with spectral and spatial resolution, we show that circular polarization in random lasers is not governed solely by intrinsic material properties. Instead, in multimode polymer optical fibers, multiple scattering produces a constrained random evolution within the guided mode space rather than unconstrained diffusion as in bulk random media. The interplay between intermode coupling, disorder induced feedback, waveguide confinement, and nonlinear gain competition dynamically selects

a limited number of effective feedback channels that function as “cavities”. Within this framework, polarization is not externally imposed but emerges as a self-organized degree of freedom associated with individual feedback configurations, providing new insight into polarization formation in disordered photonic systems and opening pathways for controlling polarization light transport without relying on material chirality.

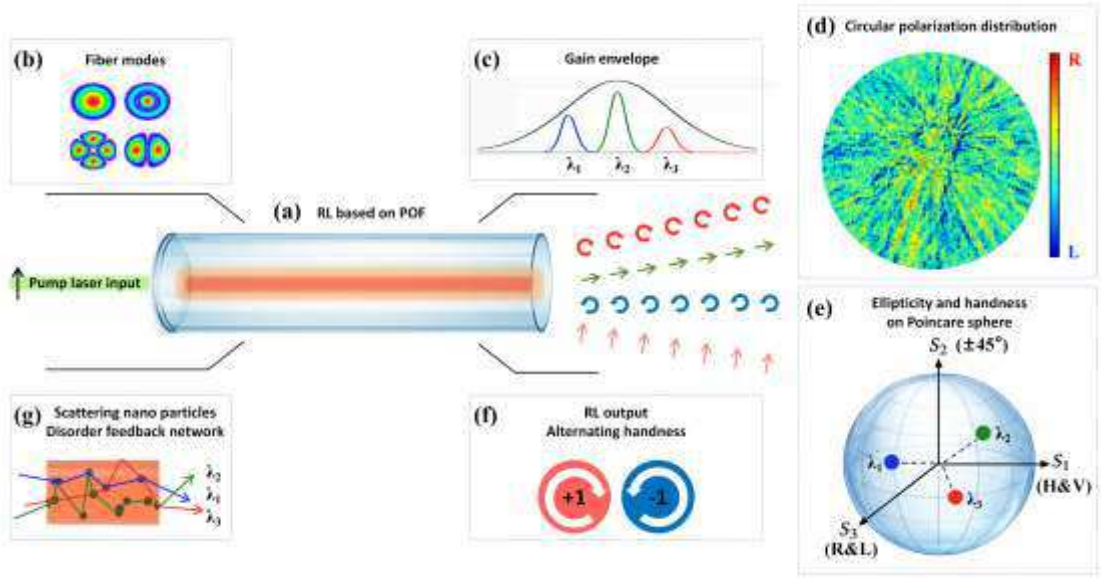


Fig. 1. Self-organization of circular polarization asymmetry in a nonchiral random fiber laser. (a) Schematic: a pump laser excites the dye-doped fiber containing scattering nanoparticles, where multimode propagation and multiple scattering form a disordered feedback network that supports random lasing. (b) Representative transverse fiber modes supported by the multimode waveguide. (c) Gain envelope of the laser dye supporting multiple lasing wavelengths (λ_1, λ_2, λ_3). (d) Spatial distribution of circular polarization across the entire output, showing mixed right-handed (R) and left-handed (L) regions. (e) Corresponding polarization states mapped on the Poincare sphere using the Stokes parameters (S_1, S_2, S_3), indicating different ellipticities and handedness for individual lasing modes. (f) Random laser emission exhibiting alternating circular polarization handedness (+1 and -1) among different lasing channels. (g) Scattering nanoparticles embedded in the dye doped polymer optical fiber create a disorder-induced feedback network through multiple scattering paths. The results demonstrate that circular polarization asymmetry can self-organize purely from disorder induced feedback without material chirality.

Results

Polarization characterization

To fully characterize the polarization state of the emitted light, we employ a complete Stokes parameter measurement scheme. The polarization state of the emitted light is

described by the four Stokes parameters S_0, S_1, S_2, and S_3. S_0 represents the total intensity, which is normalized to unity. S_1 and S_2 describe linear polarization components along orthogonal bases. S_3 quantifies the balance between right-and left-handed circular polarization components. The degree of linear polarization is defined as $D_{LP} = \sqrt{S_1^2 + S_2^2}/S_0$. The degree of circular polarization is defined as $D_{CP} = |S_3|/S_0$. The total degree of polarization is defined as $D_{OP} = \sqrt{S_1^2 + S_2^2 + S_3^2}/S_0$. These definitions are applied consistently to both spectral and spatially resolved data.

To quantify the imbalance between left and right circular polarization components, we define a circular polarization asymmetry parameter g. The parameter is defined as $g = (I_L - I_R) / (I_L + I_R)$, where I_L and I_R denote the intensities of the left-handed and right-handed circularly polarized components, respectively. In terms of the Stokes parameters, these intensities are given by $g = D_{CP} = S_3/S_0$. The asymmetry parameter g ranges from -1 to 1. The g value of 0 corresponds to perfect symmetry between left and right circular polarization, while positive and negative values indicate dominance of left-handed and right-handed circular polarization, respectively.

By measuring the spectral and spatial distributions of all four Stokes parameters, we obtain a multidimensional description of the polarization behavior. This approach allows us to track the evolution of polarization with pump energy, visualize polarization states on the Poincare sphere, and directly correlate polarization properties with specific random laser spectral modes and spatial emission channels.

To establish the noise floor of the Stokes parameter test, reference measurements were performed using a He-Ne laser and a silica fiber system under identical detection conditions. We found that a trustworthy value for D_{OP} is around 0.1, while a reasonable upper bound to the total degree of polarization, which settles around 1 for the He-Ne laser (as expected from D_{OP} definition), around 0.8 for the silica fiber, is indeed around 0.4 for the fiber with nanoparticles in the regime of multiple scattering. This behavior is expected for systems in the multiple scattering regime and for the specific detection scheme, because in the multiple scattering regime, the modes lose memory of the input polarization, which is then further averaged and mixed when coupled onto the single channel of the spectrometer. As a result, the detected signal is effectively a superposition of multiple uncorrelated polarization components, leading to a reduced D_{OP}. As we will see in the next section, the reduction of the total polarization will be even more marked in the random fiber laser. Indeed, due to multiple scattering in the gain medium, the emission consists of many lasing modes with different polarization states, and these modes are generally not phase locked. In addition, the polarization state can vary from shot to shot because of the stochastic nature of mode formation in random lasers. In our measurements, several spectra are averaged to improve the signal to noise ratio, which mixes different instantaneous polarization states and further lowers the measured D_{OP}. Other factors, such as non simultaneous polarization measurements and the collection of light over multiple spatial modes, can also introduce averaging effects that reduce the D_{OP}. Therefore, the observed D_{OP} values remaining different from unity are consistent with the partially polarized nature of the random laser emission under our experimental conditions.

Pump and wavelength resolved polarization maps under linear and circular pumping with position dependent mode and channel selection

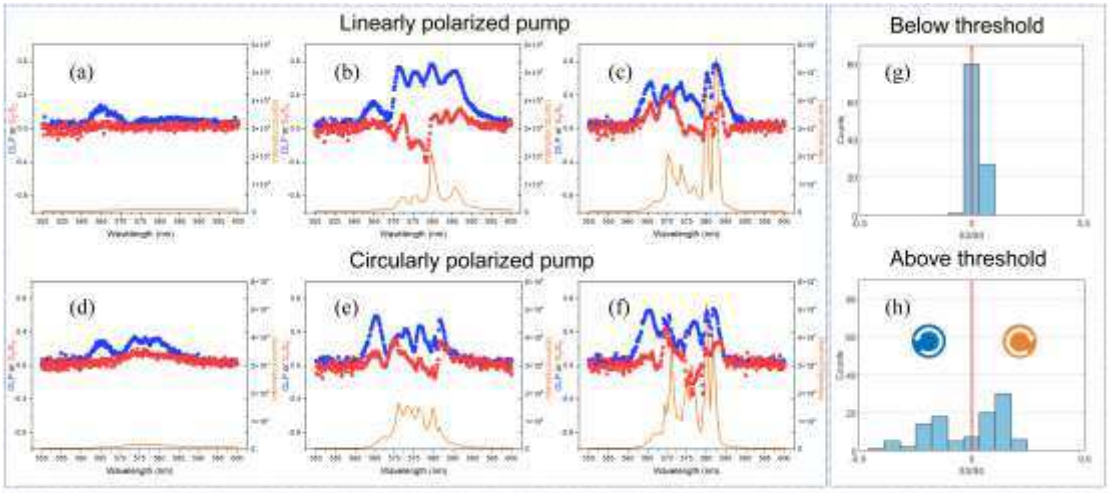


Fig. 2. Pump and wavelength resolved polarization maps under linearly and circularly polarized pumping. The orange line normalized emission intensity versus wavelength and pump energy. The blue dot is D_{LP}. The red dot is the circular component S_3/S_0. (a-c) are under linearly polarized pumping, (d-f) are under circularly polarized pumping. The pump energy is at (a,d) below the threshold, (b,e) just above the threshold, and (c,f) much above the threshold. The emergence of narrow peaks in the emission spectrum coincides with linear polarization features. The circular component exhibits mode dependent sign changes. The distribution of S3/S0 remains highly structured and does not uniformly follow the pump handedness, indicating mode selective polarization rather than trivial polarization transfer. (g,h)Statistical distribution of the Stokes parameter S_3/S_0. (g) corresponds to the below threshold regime, (h) shows the above threshold regime. Below threshold, S_3/S_0 is narrowly distributed around zero (red line), indicating no circular polarization components. Above threshold, the distribution becomes broader with enhanced fluctuations, suggesting increased S_3/S_0 and randomness.

To isolate the role of the disorder induced feedback network sketched in Fig.1(g), we first measure the emission from pure PM597 dye solutions without scattering nanoparticles as a reference. The experiment setup is shown in Fig. S2. Under optical pumping, the system exhibits spontaneous emission and amplified spontaneous emission but lacks any form of optical feedback or cavity formation. Our measurements show that emission from pure dye solutions does not exhibit any measurable circular polarization, as shown in Fig S3. This result demonstrates that in the absence of feedback, the luminescence process of PM597 alone is insufficient to generate detectable circular polarization. Any weak microscopic asymmetries are averaged out and do not survive in the far field emission, confirming that scattering feedback is essential for amplifying weak polarization asymmetries to detectable levels.

To test the mode dependent polarization selection summarized in Fig.1(f), we map

polarization across wavelength and pump energy. Fig. 2(a-c) presents pump and wavelength resolved maps of the emission intensity and polarization properties of the polymer optical fiber random laser under linearly polarized pumping. The threshold of the random laser is shown in Fig. S4. The orange lines show the emission intensity as a function of wavelength. At low pump levels, the emission is broadband and spectrally smooth, characteristic of spontaneous emission and amplified spontaneous emission. As the pump energy exceeds the threshold, discrete and spectrally localized random laser modes abruptly emerge and replace the broadband background emission, marking the onset of random lasing.

The blue dots show the corresponding D_{LP}. In the low pump regime, the D_{LP} remains small and weakly structured across the spectrum, consistent with emission dominated by spontaneous processes. Upon entering the random laser regime, clear wavelength dependent D_{LP} features appear and become increasingly correlated with the intensity maxima observed in the orange lines, indicating that polarization properties are strongly mode dependent.

The red dots show the circular polarization component quantified by the normalized Stokes parameter S_3/S_0. In contrast to intensity and linear polarization, the circular polarization map shows pronounced sign changes and localized extrema that do not simply follow the intensity distribution. Positive and negative values of S_3/S_0 coexist within the same pump condition and spectral window, often confined to narrow wavelength intervals associated with individual lasing modes.

A comparison with the lasing threshold reveals a clear transition in the circular polarization. Below the threshold, the magnitude of the third Stokes parameter remains close to zero typically within fluctuations of about ± 0.05. Above threshold, S_3/S_0 increases rapidly and stabilizes at values exceeding 0.1. This indicates that circular polarization does not gradually accumulate with increasing pump power but instead appears abruptly once the system enters the random lasing regime. This threshold associated transition can be understood from nonlinear mode selection in the multimode scattering network, as shown in Fig.1(g). In the fiber, multiple scattering continuously couples guided modes and creates many possible feedback pathways. However, due to cross gain saturation, only a limited subset of these pathways can reach threshold and remain stable. Once lasing starts, nonlinear gain competition suppresses some competing channels, allowing small polarization dependent gain differences accumulated during scattering and mode coupling to be rapidly amplified and stabilized. The polarization transition, therefore, coincides with the onset of coherent feedback rather than with a gradual increase in excitation density. In many cases, the circular polarization degree exceeds 0.1, which is well within the trustworthy measurement range. This behavior demonstrates a clear link between random lasing feedback and the generation of circular polarization, indicating that random laser dynamics play a crucial role in this process.

Fig. 2(d-f) show the corresponding pump and wavelength resolved maps obtained under circularly polarized pumping. While the intensity maps exhibit a similar transition from broadband emission to spectrally localized random lasing peaks, the overall magnitude of S_3/S_0 is enhanced. Nevertheless, the circular polarization distribution remains highly

structured, with alternating positive and negative values across both wavelength and pump energy. Notably, the handedness of the emitted circular polarization does not uniformly follow that of the pump. This result indicates that the pump polarization modifies the gain balance but does not uniquely determine the polarization state of individual random laser modes.

As shown in Fig.2(g,h), we analyzed the statistical distribution of S_3/S_0 around the random laser threshold. Below the threshold, the S_3/S_0 values are tightly concentrated near zero, with a small distribution range, indicating the absence of circular polarization and relatively stable linear polarization behavior. Above the threshold, the distribution becomes wider and more dispersed, with circular polarization components appearing and fluctuating. This change clearly shows that the circular polarization component increases significantly once random laser emission begins.

Mode and channel dependence under controlled pump position

A key finding of this work is that circular polarization is not uniform across the emission spectrum or spatial profile. Instead, the degree and handedness of circular polarization are closely associated with specific random laser spectral modes and spatial emission channels.

To investigate how the local excitation condition influences polarization selection in the disordered fiber feedback network, we performed linearly polarized pumping at two lateral positions relative to the fiber core, slightly offset to the left and to the right of the center. In Fig. 3, for both pumping positions, the intensity maps display the typical evolution from broadband emission at lower pump energies to spectrally localized emission bands and narrow high-intensity peaks at higher pump energies. This behavior indicates that random lasing feedback is established in both cases. However, the detailed spectral trajectories of the dominant intensity bands differ between the two positions. These differences show that even small shifts in pump position can redistribute the effective gain and scattering feedback pathways, thereby selecting different subsets of random lasing modes.

The D_{LP} dots further reveal that linear polarization is strongly mode dependent and sensitive to pumping position. Under both pumping conditions, elevated D_{LP} values appear mainly in the same spectral regions that host the dominant intensity features. This correlation confirms that the polarization state is associated with specific lasing channels rather than with the overall fluorescence background. Most importantly, the S_3/S_0 dots demonstrate that circular polarization under linearly polarized pumping is not uniform across the fiber and is highly sensitive to the local excitation geometry. Although both positions exhibit finite S_3/S_0 values that mainly appear in the random laser regime, the spectral positions and sign distribution of S_3/S_0 differ significantly. This difference indicates that both the handedness and magnitude of circular polarization are not fixed material properties. Instead, they are determined by the specific scattering trajectories and interference conditions activated by the local pump position. Taken together, the comparison between the two off center pumping positions provides direct evidence that circular polarization asymmetry in this nonchiral random

laser is channel selective and spatially heterogeneous, meaning that circular polarization arises from self-organized mode competition within a disordered feedback network rather than from polarization transfer from the pump.

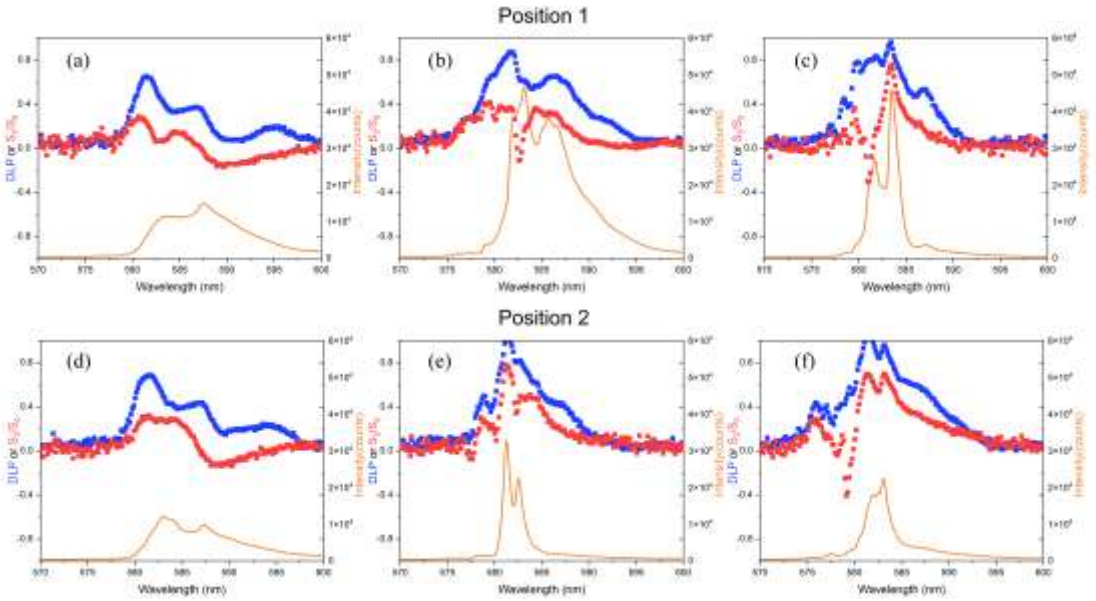


Fig. 3. Pump position dependence under linear polarization pumping. The figure shows the emission intensity, D_{LP}, and S_3/S_0 as a function of wavelength for two transverse pump positions relative to the fiber core. (a-c) represents position 1, and (d-f) represents position 2. The pump energy is at (a, d) below the threshold, (b, e) just above the threshold, and (c, f) much above the threshold. The mode trajectory and S_3/S_0 change with pump position, indicating the existence of channel selective polarization selection.

This behavior cannot be explained by intrinsic molecular properties of the dye, which are identical throughout the sample. Instead, each lasing mode corresponds to a distinct effective feedback channel involving different combinations of guided modes and scattering paths. These differences naturally lead to different accumulated phase and gain conditions for orthogonal polarization components.

It is worth noting that the magnitude of S_3/S_0 in Fig. 3 is clearly higher than that observed in Fig. 2. This difference is mainly related to the excitation geometry and the resulting mode selection in the disordered fiber. In Fig. 2, the pump is more symmetric with respect to the fiber, so a larger number of modes and feedback channels are simultaneously excited. The detected signal, therefore, contains contributions from many channels with different polarization states, and the circular components tend to partially cancel each other, leading to relatively smaller S_3 values.

In contrast, in Fig. 3, the pump is intentionally shifted off center, which breaks the symmetry of the excitation and restricts the set of active modes. Under these conditions, only a smaller number of feedback channels dominate the emission. Since each channel carries its own polarization state, reducing the number of contributing channels also reduces the averaging between opposite circular components. As a result, any imbalance between the two circular polarizations becomes more visible, leading to a

larger measured S_3/S_0. This comparison indicates that the magnitude of S_3/S_0 is not only determined by the intrinsic properties of the system, but also strongly influenced by how many modes and channels are involved in the emission and how they are spatially excited.

At some peak positions, the calculated D_{OP} is slightly larger than 1. This reflects the uncertainty of the Stokes reconstruction since the excitation of random laser leakage modes. The emission intensity changes from shot to shot (with respect to the optimal pumping condition), exciting leakage modes of the fiber that strongly affect the collection of the emitted light, eventually affecting the parameters for Stokes reconstruction.

Spatial channel selectivity and pixel level correlation

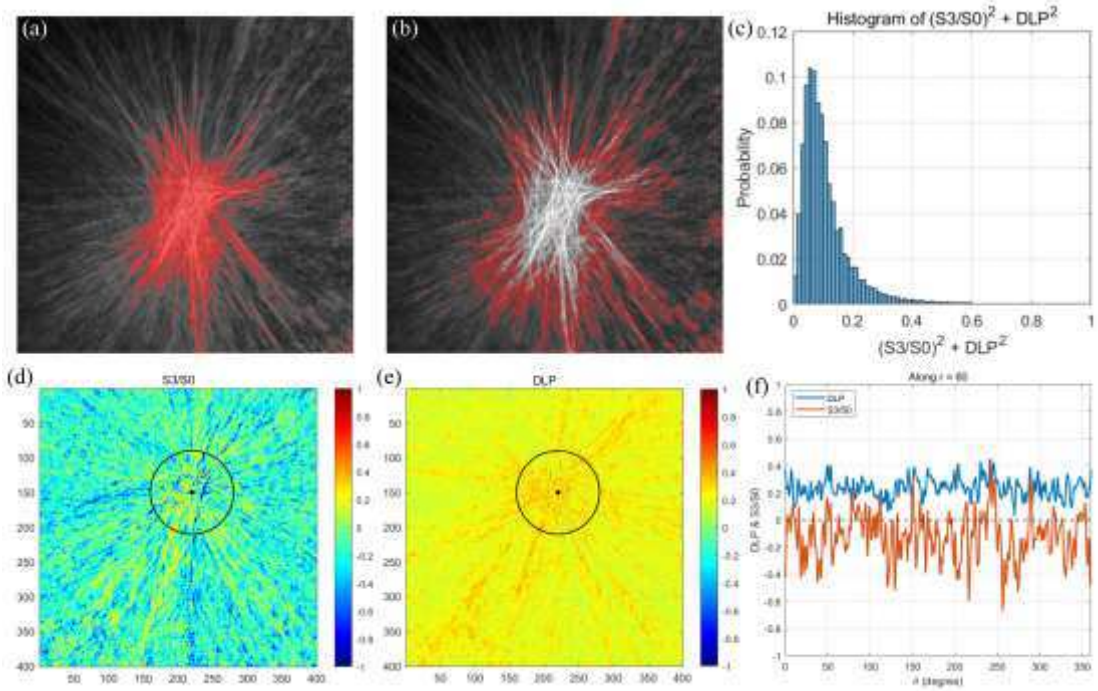


Fig. 4. Spatially resolved polarization analysis. Red pixels show (a) the top 10% of emission intensity, (b) the top 10-20% of emission intensity. (d) S_3/S_0 and (e) D_{LP} spatial maps in the emission spot. (f) Angular dependence of D_{LP} and S_3/S_0 at a fixed radius r=60 pixels, showing D_{LP} (blue) and S_3/S_0 (orange) as a function of the azimuthal angle θ. The calculated circle is marked in (d) and (e). (c) Probability histogram of D_{OP} extracted from the random laser emission image. The D_{LP} remains relatively smooth and positive, whereas S_3/S_0 exhibits strong fluctuations and frequent sign reversals, indicating angle dependent switching of circular polarization handedness along the circular path.

To link the spatial domains shown in Fig.1(d) to specific emission channels and identify the spatial origin of the observed polarization selectivity, we reconstruct pixel-by-pixel Stokes parameters and analyze the spatially resolved emission patterns. Fig. S4(a-e) show spatial emission images used to reconstruct the full Stokes parameters of the

polymer optical fiber random laser. The intensity percentile maps in Fig. 4(a,b) further reveal the spatial hierarchy of emission channels. The left panel highlights the pixels within the top 10% of emission intensity, which are concentrated in a small number of dominant filamentary paths. When the threshold is relaxed to include the top 20% of pixels, the emission gradually extends into surrounding weaker channels while maintaining the same overall radial structure. This progressive spatial broadening indicates that the strongest emission originates from a limited subset of highly selected feedback paths, whereas weaker occupies a larger portion of the disordered network. The comparison between intensity percentile maps and the polarization resolved analysis shows that strong polarization effects are spatially localized within these dominant emission channels rather than being uniformly distributed across the emission area.

Fig. 4(d,e) examine the spatial distribution of polarization within the random laser emission spot. The overview image defines a central region of interest, and the accompanying maps show S_3/S_0 and D_{LP}. In the S_3/S_0 map, these filaments are not uniform. Neighboring streaks often switch between positive and negative values, which means the handedness of the circular component alternates across adjacent emission channels. The D_{LP} map peaks along the same bright filaments and remains lower in the surrounding diffuse background. This correspondence indicates that the most intense structures are also the most strongly polarized.

The central region contains bundles of thin filaments that preserve their sign of S_3/S_0 over tens of pixels before switching at filament boundaries. Along individual filaments, the D_{LP} increases gradually and reaches local maxima where the grayscale image shows the strongest intensity contrast. In contrast, regions between filaments show reduced D_{LP} together with rapidly fluctuating S_3/S_0, indicating weaker and less ordered polarization states.

Fig. 4(f) shows the angular dependence of D_{LP} and S_3/S_0 at a fixed radius r=60 pixels. The D_{LP} remains relatively stable over the full angular range, with values typically between 0.2 and 0.4, indicating a persistent but moderately varying linear polarization component along the selected circular path. In contrast, S_3/S_0 exhibits strong fluctuations with frequent sign reversals, spanning a broad range from negative to positive values. This behavior reveals that the circular polarization component is highly angle dependent and alternates in handedness as a function of θ. The coexistence of a relatively smooth D_{LP} profile and a strongly oscillatory S_3/S_0 suggests that linear and circular polarization components evolve largely independently along the radial direction, reflecting the complex interference and mode dependent polarization selection within the disordered feedback network.

Fig.4 (c) shows the histogram of $((S3/S0)^2 + D_{LP}^2)$ extracted from the random laser emission image. The distribution is strongly concentrated in the low value region, with a peak around 0.1, and decays rapidly as the value increases, exhibiting a clear right skewed behavior. The average value of the distribution is 0.1, and most pixels have values below 0.3, while occurrences near 1 are rare. This indicates that the emission from the random laser is predominantly weakly polarized, with only a small fraction of localized regions showing relatively higher polarization. Such a distribution is

consistent with the test that we show in Fig S1, which is supposed to be smaller than in the case of fiber with nanoparticles, the D_{OP} is around 0.4.

These spatially resolved polarization images show that the random laser emission from the fiber is not uniform but divided into alternating circular polarization domains embedded within regions of strong linear polarization. The center of the emission spot displays pronounced elliptical polarization, which means that both the linear and circular components contribute significantly. Such behavior is expected when interference between multiple lasing modes converts linear polarization into circular components. The same alternation pattern appears both across the full image and in the magnified central regions. This observation indicates that the polarization structure originates from multimode interference and polarization mixing inside the disordered waveguide rather than from slow spatial variations of the sample itself.

Pixel level correlation analysis further clarifies the relationship between circular and linear polarization. As shown in Fig. S5(f), the circular and linear polarization components evolve largely independently across the emission field. Such behavior suggests that polarization formation in the random laser cannot be described by a simple conversion between linear and circular polarization. Instead, the polarization state is determined by the specific modal and scattering feedback pathways within the disordered multimode fiber.

Taken together, the multiscale maps reveal a consistent coupling between emission intensity and polarization order. High-gain channels concentrate both the linear and circular components, while the handedness of the circular component varies from channel to channel. This behavior demonstrates that the preferential propagation paths of the random laser carry spatially structured elliptical polarization rather than a uniform polarization state.

Self-organization of polarization states on the Poincare sphere

Following the representation in Fig.1(e), we represent polarization states by normalized Stokes vectors (S_1/S_0, S_2/S_0, S_3/S_0) and visualize their distributions on the Poincare sphere as pump energy increases in Fig. 5(a-g). Below threshold, the point cloud is mainly confined near the equator, and the spread in S_3 is small, indicating a negligible circular polarization component. As the pump approaches and exceeds threshold, the distribution expands into three dimensions, with a clear increase in the spread along S_3. This behavior suggests that circular polarization becomes active and evolves as an additional, independent degree of freedom. In a disordered system, multiple scattering together with finite geometry forms a complex network of optical paths. Along these paths, even weak polarization dependent effects, such as gain anisotropy or scattering anisotropy, can accumulate and produce small differences between the left and right circular components. Such imbalances can then appear as an enhanced spread or asymmetry on the Poincaré sphere.

To quantify how the polarization distribution evolves, we extracted several statistical metrics from the measured Stokes point clouds under different pump conditions for S_3/S_0, which is also g. First, to characterize strong circular polarization while reducing

sensitivity to isolated outliers, we compute robust circular polarization metrics: the maximum and the 95th percentile of $|S_3/S_0|$.

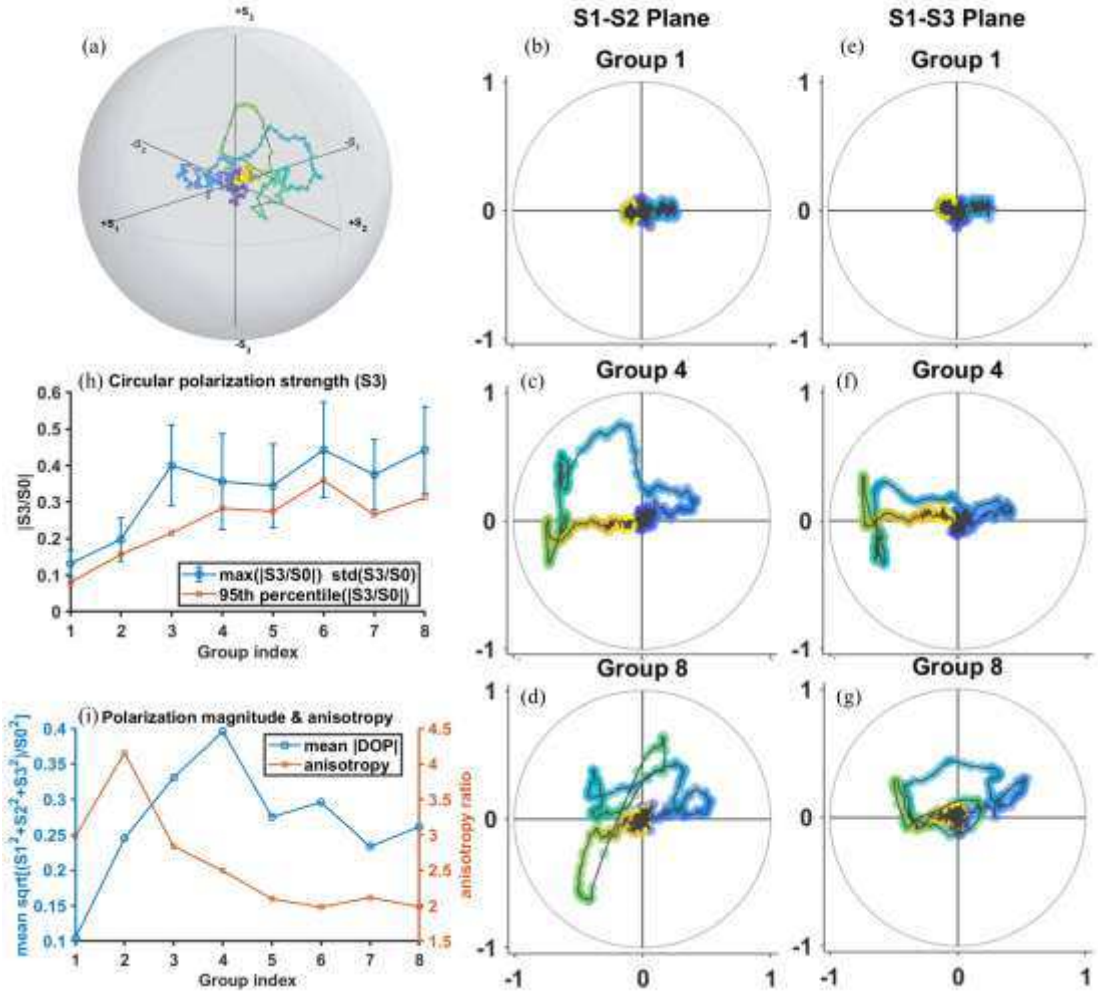


Fig. 5. Evolution of polarization state distributions with pump energy. (a) The normalized Stokes point cloud on the Poincare sphere for high pump energy. The 2D distribution of the point cloud on the (b-d) S_1-S_2 plane and (e-g)S_1-S_3 plane of the Poincare sphere. Group 1-8 indicate the lowest pump energy to the highest pump energy. The pump energy is (b,e) below the threshold, (c,f) just above the threshold, and (d,g) much above the threshold. (h, i) Statistical metrics of polarization state distributions versus pump energy group. Metrics include (h) max(|g|), 95th percentile(|g|); (i) mean D_{OP}, and anisotropy parameter. The onset of random lasing coincides with expansion along g and increased 3D of the polarization distribution.

To describe the anisotropy of the polarization distribution on the Poincare sphere in a more quantitative way, we evaluate the spread of the normalized Stokes components along each axis. Specifically, we calculate the standard deviations σ_1, σ_2, and σ_3 of S_1/S_0, S_2/S_0, and S_3/S_0 over all measured points. The anisotropy parameter A is then defined as the ratio between the largest and the smallest of these values, $A = \max(\sigma_1, \sigma_2, \sigma_3) / \min(\sigma_1, \sigma_2, \sigma_3)$. This definition reflects how uneven the distribution is along different directions. If the polarization states are distributed similarly along all three axes, A is close to 1, corresponding to a nearly isotropic distribution. If one direction is more

pronounced, A increases, indicating that the distribution is stretched along that specific Stokes component. In practice, this allows us to distinguish between a distribution mainly confined near the equatorial plane (weak S_3 component) and a more extended 3D distribution where the circular component becomes significant.

As summarized in Fig. 5(h, i), both maximum and 95th percentile values of $|g|$ increase markedly from Group 1 to Group 3 as the pump energy increases. This indicates that a pronounced circular polarization asymmetry emerges once coherent random lasing feedback is established. The decrease of anisotropy A, from values larger than 4 to values approaching 2, indicates that the polarization distribution becomes progressively more isotropic. This means that the asymmetry parameter *g* is no longer strongly constrained, and the polarization states move away from a distribution mainly confined to the equatorial plane of the Poincare sphere. The mean degree of polarization D_{OP} increases rapidly near the lasing threshold and reaches a maximum at intermediate pump levels, reflecting enhanced polarization coherence during the onset of random lasing. At higher pump powers, it decreases slightly, which is consistent with stronger mode competition and increased polarization mixing among simultaneously excited modes.

Below the lasing threshold, the circular polarization asymmetry g remains negligible. Once the threshold is exceeded, mode competition selectively amplifies certain scattering paths while suppressing others, leading to the self-organization and stabilization of specific polarization states with nonzero g. Under these conditions, the random laser can be interpreted as an asymmetric optical cavity that responds differently to the two circular polarization components, even though the material itself is not chiral. The observed circular polarization asymmetry therefore originates from disorder induced optical feedback and mode selection, rather than from any intrinsic structural handedness. As a result, the feedback process gives rise to spontaneous polarization symmetry breaking.

Discussion

We have demonstrated the emergence of pronounced circular polarization and circular polarization asymmetry in a completely nonchiral random laser system based on polymer optical fibers. Pure dye emission without scattering feedback exhibits negligible circular polarization, while the onset of random fiber lasing leads to the abrupt appearance of circular polarization components above threshold. Through full Stokes parameter characterization with spectral and spatial resolution, we show that circular polarization is correlated with individual random laser modes and spatial emission channels, with different modes exhibiting distinct ellipticities and even opposite handedness.

These observations can be understood by considering the multimode waveguiding and disorder induced feedback structure of the polymer optical fiber system. The fiber provides a finite waveguide that supports a large set of guided electromagnetic modes under the fiber boundary conditions. The embedded scattering nanoparticles introduce

multiple scattering events that continuously couple, redistribute, and reorganize these guided modes. As a result, light propagation in the system is not an unconstrained random walk as in bulk scattering media, but a constrained random evolution within the modal space of the multimode waveguide. Within this modal space, certain combinations of scattering paths and mode coupling form effective feedback channels that behave as dynamically established high Q configurations in the scattering network and act as effective cavities for random lasing. The random laser can be viewed as a multimode nonlinear system in which frequency modes, spatial channels, and polarization states are jointly selected through disorder induced feedback and gain competition.

Because different lasing modes partially share the available gain, nonlinear effects such as gain saturation and mode competition limit the number of feedback configurations that can reach threshold simultaneously, although many possible scattering trajectories exist in the fiber, only a small subset of configurations is selected by the combined action of multiple scattering, multimode dispersion, and nonlinear gain competition, establishing a feedback network that is generally not equivalent for the two circular polarization components at the level of individual lasing trajectories.

Along these effective feedback trajectories, repeated scattering, intermodal coupling, and reflections at the core cladding boundary introduce polarization rotation, mixing, and phase accumulation. Consequently, the two orthogonal polarization components generally experience slightly different effective gain and phase conditions after one feedback cycle. Once the random laser threshold is exceeded, however, nonlinear amplification rapidly enhances even minute gain differences.

Within this framework, polarization selection can be viewed as an extension of random laser mode competition into the polarization degree of freedom. Different spectral modes correspond to different effective feedback configurations and modal participation ratios, thus leading to different Stokes vectors. This naturally leads to mode dependent polarization states with distinct ellipticity and handedness. Because different spatial emission filaments correspond to different local feedback networks, the amplification imbalance between the two circular polarization components may even reverse sign from one channel to another, producing the experimentally observed alternation of circular polarization handedness across neighboring spatial channels.

From this perspective, the threshold associated emergence of circular polarization, together with its mode and channel dependent behavior, reflects the self-organized selection of polarization states within a random multimode feedback network. Random lasing thus acts as an effective asymmetric optical cavity that stabilizes small polarization asymmetries through nonlinear amplification. These results reveal that disordered photonic systems can spontaneously generate circular polarization asymmetry even in the absence of material chirality, providing new insight into polarization dynamics in random lasers and opening opportunities for controlling light based on its polarization state in disordered gain media.

Materials and methods

Polarization properties of PM597

PM597 is a laser dye with a well-defined linear electronic transition dipole moment approximately aligned along the molecular long axis. As a result, absorption and stimulated emission cross sections are anisotropic with respect to linearly polarized excitation. This anisotropy can lead to polarization dependent gain under linearly polarized pumping, particularly in media where molecular rotation is restricted.
In low viscosity isotropic solvents, PM597 molecules undergo rapid rotational diffusion on timescales much shorter than the fluorescence lifetime. Under such conditions, any excitation induced polarization memory is averaged out, and the emitted fluorescence is only weakly polarized. In contrast, when PM597 is embedded in solid or semisolid matrices such as polymer optical fibers, rotational freedom is partially suppressed. This suppression can preserve linear polarization anisotropy in emission and amplified spontaneous emission.
Importantly, PM597 is achiral and does not possess an intrinsic mechanism for generating circular polarization asymmetry. In the absence of polarization selective optical feedback, emission from PM597 does not exhibit a systematic preference between left and right-handed circular polarization components. Consequently, any measurable circular Stokes component observed in the present experiments must originate from the optical feedback environment rather than from intrinsic molecular chirality.

Polymer optical fiber

The random laser system investigated in this work consists of a polymer optical fiber doped with the laser dye PM597 and scattering nanoparticles based on iron oxide@silica core&shell structures. The fiber used in the experiment is 5cm long. The polymer optical fiber provides a finite and weakly guiding geometry that confines light while remaining intrinsically nonchiral. The embedded nanoparticles introduce strong elastic scattering, enabling the formation of closed or quasi closed optical paths required for random lasing. Together, finite geometry and multiple scattering define a disordered optical feedback network without mirrors or designed resonant structures.

Acknowledgements

This work was supported by the Misura e controllo ottico di fenomeni fisici (DFM.AD005.426.001), the Air Force Office of Scientific Research (FA8655-24-1-7005). The authors would like to thank Professor Nicolas Cherroret for all the insightful

advice on this paper and Professor Walter Margulis for the nice discussion on fiber polarization.

Data availability

The data that support the findings of this study are available from the corresponding author upon reasonable request.

Conflict of interest

The authors declare no competing interests.

References

[1] Letokhov, V. S. Optical generation by a scattering medium with negative resonance absorption. *FTDMT2411268* (1968).
[2] Lawandy, N. M., Balachandran, R. M., Gomes, A. S. L. & Sauvain, E. Laser action in strongly scattering media. *Nature* **368**, 436–438 (1994).
[3] Wiersma, D. S. The physics and applications of random lasers. *Nat. Phys.* **4**, 359–367 (2008).
[4] Cao, H. Lasing in random media. *Waves Random Media* **13**, R1–R39 (2003).
[5] Gomes, A. S. L., Moura, A. L., Araújo, C. B. & Raposo, E. P. Recent advances and applications of random lasers and random fiber lasers. *Prog. Quantum Electron.* **78**, 100343 (2021).
[6] Ignesti, E. et al. Experimental and theoretical investigation of statistical regimes in random laser emission. *Phys. Rev. A* **88**, 033820 (2013).
[7] van der Molen, K. L., Mosk, A. P. & Lagendijk, A. Intrinsic intensity fluctuations in random lasers. *Phys. Rev. A* **74**, 053808 (2006).
[8] Gottardo, S., Sapienza, R., Garcia, P. D., Blanco, A., Wiersma, D. S. & López, C. Resonance-driven random lasing. *Nat. Photon.* **2**, 429–432 (2008).
[9] Leonetti, M., Conti, C. & López, C. The mode-locking transition of random lasers. *Nat. Photon.* **5**, 615–617 (2011).
[10] Knitter, S., Kues, M. & Fallnich, C. Emission polarization of random lasers in organic dye solutions. *Opt. Lett.* **37**, 3621–3623 (2012).
[11] Ye, L., Feng, Y., Yang, S. & Xu, H. Study on the polarization of random lasers from dye doped nematic liquid crystals. *Nanoscale Res. Lett.* **12**, 27 (2017).
[12] Leonetti, M., Conti, C. & López, C. Random laser tailored by directional stimulated emission. *Phys. Rev. A* **85**, 043841 (2012).
[13] Ji, M. J. et al. Circularly polarized luminescence with high dissymmetry factors for achiral organic molecules in solutions. *Nat. Commun.* **16**, 2940 (2025).

[14] Liu, J. J. et al. Enhancing circularly polarized luminescence in chiral fluorescent dyes via cholesteric liquid crystal polymer networks. *ACS Appl. Polym. Mater*. **7**, 4029–4037 (2025).
[15] Zheng, H. R. et al. Rational design of circularly polarized luminescence active chiral metal organic frameworks for logic devices. *Chem. Sci.* (2025).
[16] Yao, K. et al. Excitation dependent circularly polarized luminescence inversion driven by dichroic competition of achiral dyes in cholesteric liquid crystals. *Angew. Chem.* **137**, e202420290 (2025).
[17] Lin, L. Z. et al. Circularly polarized stimulated emission from a chiral cavity based on apparent circular dichroism organic thin films. *ACS Photonics* **12**, 2557–2565 (2025).
[18] Leonetti, M., Conti, C. & López, C. Random laser tailored by directional stimulated emission. *Phys. Rev. A* **85**, 043841 (2012).
[19] Lee, S., Kim, H. & Jeong, Y. Angular distribution of luminescence dissymmetry observed from a random laser built upon the exocuticle of the scarab beetle Chrysina gloriosa. *Opt. Express* **29**, 37712–37721 (2021).
[20] Lee, S. et al. Random lasing with a high degree of circular dichroism by chiral plasmonic gold nanoparticles. *ACS Photonics* **9**, 613–620 (2022).

Supplementary Files

This is a list of supplementary files associated with this preprint. Click to download.

- SIwenyu.docx